Terahertz microcavity lasers with subwavelength mode volumes and thresholds in the milliampere range

Y. Chassagneux, J. Palomo, and R. Colombelli[a)]
Institut d'Electronique Fondamentale, Université Paris Sud, CNRS, 91405 Orsay, France

S. Dhillon and C. Sirtori
Matériaux et Phénomènes Quantiques, Université Paris 7, 75251 Paris, France

H. Beere, J. Alton, and D. Ritchie
Cavendish Laboratory, University of Cambridge, Cambridge CB3 OHE, United Kingdom

(Received 4 January 2007; accepted 29 January 2007; published online 1 March 2007)

The authors demonstrate terahertz microcavity lasers with ultralow current thresholds ($I_{th} \approx 4$ mA) and with reduced mode volumes of $\approx 0.7(\lambda_{effective})^3$, i.e., less than one cubic wavelength. A double metal waveguide with reduced active core thickness (5.82 μm) is used to achieve confinement in the vertical direction, without compromising the laser performances. Confinement in the longitudinal direction is obtained using microdisk resonators. The guiding properties of surface plasmons are exploited to guide the mode with the metal contact. This makes the use of a resonator with vertical and smooth sidewalls unnecessary. The emission wavelength is $\lambda \approx 114$ μm. The devices lase up to 70 K in pulsed mode, and they achieve continuous-wave operation up to 60 K. © *2007 American Institute of Physics*. [DOI: 10.1063/1.2710754]

Terahertz quantum cascade (QC) lasers are semiconductor-based sources of coherent radiation covering the frequency range between 1.9 and 5 THz ($\lambda \approx 60-160$ μm).[1,2] They are the only compact sources of coherent radiation in this wavelength range. The numerous applications of terahertz radiation (imaging, spectroscopy, and biosensing[3]) have recently triggered much interest on these lasers.

An efficient waveguide used for these devices is based on the metal-metal geometry, where the mode confinement is provided by a double-sided metal coating.[4,5] Metal-metal waveguides offer near unity confinement factors (Γ) with limited propagation losses. The extreme mode confinement in the vertical direction suggests the realization of devices where a similar extreme confinement is present in the lateral/planar directions, with a twofold motivation.

On one hand, devices with small surfaces allow for very low current thresholds (I_{th}) for laser oscillation, making the power-dissipation requirements less stringent. Their emission is typically single mode, since the number of modes that overlap with the material gain spectrum is reduced. The limited output power constitutes a drawback, but for certain applications (local oscillators, for example) a few tens of microwatts represent an acceptable power level. However, there are also more fundamental reasons. In the domain of semiconductor physics, a definite trend is present towards the implementation of "nanocavities,"[6] whose volume is small enough to control the spontaneous emission. This is potentially interesting for *interband* lasers, since they emit a large amount of undesired spontaneous emission before lasing, which degrades their efficiency.[7] This principle is not applicable to lasers based on *intersubband* (ISB) transitions, since nonradiative processes (LO-phonon and electron-electron scatterings) are the limiting factors to the device efficiency. The spontaneous emission rates (Γ_{rad}) can be tailored via the photonic density of states, but a change in Γ_{rad} has an irrelevant effect on the laser threshold current. Despite this, metal-metal λ-sized cavities for terahertz emitting devices can play a major role for the study of strong-coupling effects. In a microcavity (in the absence of population inversion[8]), if the coupling between the electronic transition and the cavity photon mode is faster than the damping rates, new normal modes—called microcavity polaritons—may arise. In particular, in the terahertz, it has been recently proposed[9] that an unexplored *ultrastrong*-coupling regime could be obtained, when the Rabi frequency becomes comparable to the energy of the ISB transition.

In this letter, we demonstrate terahertz microcavity QC lasers with ultralow current thresholds. The laser resonator is based on a microcylindrical geometry, already successfully used in the mid-IR,[10] and its effective mode volume is $\approx 0.7(\lambda/n_{eff})^3$, where λ is the emission wavelength in the vacuum and n_{eff} is the mode effective refractive index. The extreme confinement in the vertical direction (**z**, see Fig. 1) is obtained using a metal-metal waveguide, while in the planar directions (**x**,**y**) the guiding properties of surface plasmons are exploited.[11,12] Note that a wavelength-sized spatial confinement in all three dimensions is possible, thanks to the use of a metal-metal waveguide. In this geometry Γ remains always close to unity, regardless of the active region thickness. This is not the case for a regular dielectric[13] or even for semiconductor-slab waveguides.[14] Also, an extreme lateral confinement in a dielectric waveguide geometry effectively "pushes" the mode into the substrate, thus canceling the effect of the strong localization in the **x**-**y** plane.

The sample was grown by molecular beam epitaxy, with active core thickness of 5.86 μm (45 active core/injector stages). The active region, designed for emission at 2.9 THz (12 meV), is described in Ref. 15. It is sandwiched between 700 nm, 2×10^{18} cm^{-3} and 80 nm, 5×10^{18} cm^{-3} doped layers forming the lower and upper contacts. The QC wafer was thermocompressively bonded onto a *n*-GaAs wafer. After selective etching, the 700-nm-thick top doped layer was thinned to 200 nm to reduce free carrier absorption. Devices fabricated in a ridge waveguide geometry lase in cw (T_{max}

[a)]Electronic mail: colombel@ief.u-psud.fr

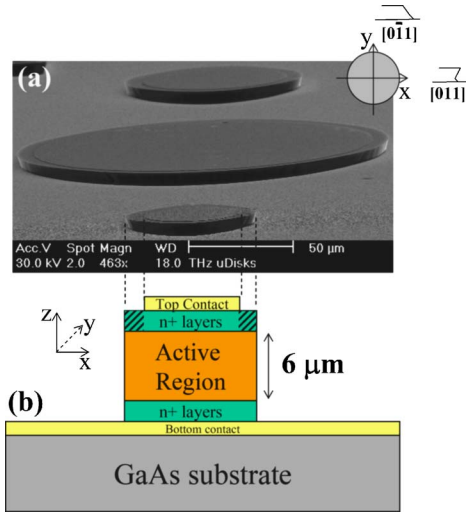

FIG. 1. (Color online) (a) Scanning electron microscope image of the fabricated microdisks. The sidewalls are not vertical and their slope depends on the crystal orientation, as shown in the top-right schematic drawing. (b) Schematic device geometry before the removal of the top n^+ doped layers. The metal top contact does not cover the whole top surface of the microcylinder. Radii of the fabricated microdisks: 32/45/95 μm. Radii of the deposited metal: 25/37.5/87.5 μm. The hatched regions are the portions of n^+ layer that are removed to increase the resonator Q factor.

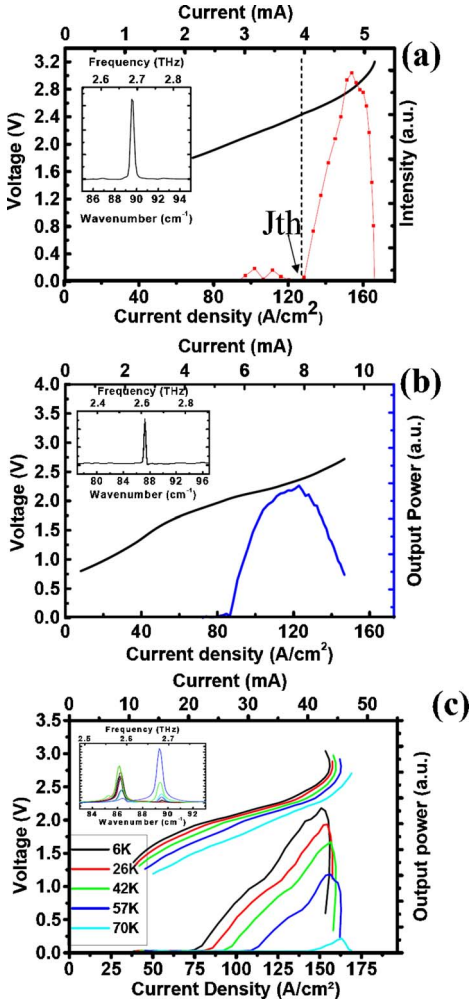

FIG. 2. (Color online) (a) (LVI) characteristics at 6 K and in cw mode of a typical small-size (r=25 μm) terahertz microdisk. The I_{th} is ≈4 mA. Inset: emission spectrum at 6 K for an injection current of 4.75 mA. The detection was performed with a He-cooled silicon bolometer. (b) LVI characteristics at 6 K and in cw mode of a typical medium-size (r=37.5 μm) terahertz microdisk. The I_{th} is ≈5.5 mA. Inset: emission spectrum at 6 K for an injection current of 8 mA. (c) LVI characteristics at several temperatures and in pulsed mode (300 ns at 20 kHz) of a typical large-size (r=87.5 μm) terahertz microdisk. The I_{th} at 6 K is ≈21 mA and the devices operate up to 70 K. Inset: emission spectra for several injection currents.

=60 K) and pulsed (T_{max}=75 K) modes, with a threshold of 71 A/cm^2 at a temperature of 10 K.[16]

The microresonators for this work were fabricated as follows. Circular microdisks with three different radii (r=32, 45, and 95 μm, respectively) were etched down to the bottom wafer-bonded Ti/Au layer. In Ref. 17 terahertz microdisk lasers were realized using an inductively coupled plasma reactive ion etching to achieve vertical walls. Here, an anisotropic H_2SO_4-based wet etch was used, which results in nonvertical sidewalls with angles dependent on the crystal orientation (Fig. 1). The top metallic contacts (Cr/Au, 10/200 nm) have radii of 25, 37.5, and 87.5 μm, respectively. The contacts are smaller than the resonators, as shown in Figs. 1(a) and 1(b). This was done intentionally in order to cancel the negative effect of the nonvertical sidewalls. Ideally, in fact, the optical mode is guided by the top metal contacts, without being affected by the irregular shape of the microresonator. This geometry also makes the use of reactive-ion-etch techniques unnecessary. It is crucial to remove the n^+ contact layer between the top metal border and the edge of the disk [Fig. 1(b), hatched regions] in order to prevent the optical mode from being guided by the very lossy, highly doped semiconductor.

The devices were mounted in a He-flow cryostat for electro-optical characterizations. Prior to the removal of the top n^+ layer [Fig. 1(b)], the devices were not achieving laser threshold. The sample was then briefly dipped into a sulfuric acid solution to remove the top doped layers. Devices were functioning after this operation. The results are reported in Fig. 2. The I_{th} do not change between pulsed and cw modes, but the T_{max} in the former case is 70 K, while in the latter one it is 60 K. The smallest devices with r=32 μm [Fig. 2(a)] exhibit an I_{th} of ≈4 mA in cw at 10 K, with a single-mode emission peaked at ≈89.5 cm^{-1} (λ=111.7 μm). The J_{th}—calculated under the approximation that the current spreads across the whole device volume—is ≈125 A/cm^2. The medium-sized devices with r=45 μm [Fig. 2(b)] are single mode too, with a peak emission at ≈88 cm^{-1} ($\lambda \approx 113.6$ μm). The I_{th} in cw at 10 K is 5.5 mA, corresponding to a lower J_{th} of ≈87 A/cm^2. Finally the larger devices with r=95 μm exhibit an I_{th} of ≈21 mA, corresponding to an even lower J_{th} of 74 A/cm^2. Figure 2(c) reports a complete light-voltage vs current (LVI) characterization of a typical device in pulsed mode at different temperatures. Contrary to the smaller devices, the emission spectrum is bimodal (λ=116 μm and λ=112 μm). All the lasers were measured as edge emitters, but similar signal intensities were detected from the surface. The approximation that the current spreads across the whole device volume is validated by the observation that the *IV* characteristics of devices with different sizes overlap if the *whole resonator surface* (and not the top contact surface) is used to calculate the current density.

In order to interpret the spectral properties of the small-size microdisks, three-dimensional (3D) simulations of the resonator modes were performed within a finite-element (FE) approach.[19] The numerical problem was simplified by neglecting the thin n^+ doped contact layers on both sides of the

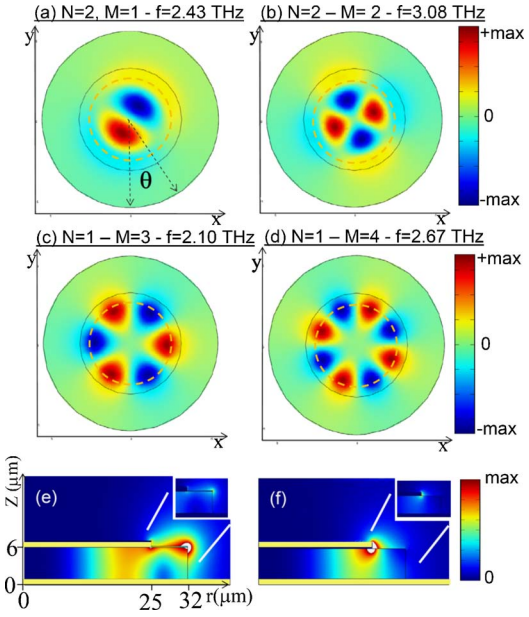

FIG. 3. (Color online) Numerical simulations of the modes in the microcylinder devices with the smallest diameter. The 3D simulations are performed within a finite-element approach (Ref. 18). For the 2D simulations we have mapped the 3D problem onto a 2D one using the axial symmetry of the system, as described by Oxborrow in Ref. 19. [(a)–(d)] 3D simulations of the modes with radial numbers $N=1,2$ and azimuthal numbers $M=1$, 2, 3, and 4. The vertical component E_z of the electric field on a horizontal section is plotted. The dotted circles correspond to the extension of the metal contact. The mode is bound to the metal and the resonance frequencies—reported on the panel legends—are spaced of ≈0.3 THz. The lasing mode is $N=1$, $M=4$ (d). (e) Axisymmetric simulation of the ($N=1$, $M=4$) mode prior removal of the n^+ top doped layer. The electric field magnitude $|\mathbf{E}|$ is plotted. The mode is guided by the top n^+ layer up to the resonator edge. Inset: close-up of the mesa edge with a three-times larger color scale. It shows that the white region in the main picture is not a numerical divergence but just out of scale. (f) Axisymmetric simulation of the ($N=1$, $M=4$) mode after the removal of a part of highly doped layer. The mode is now bound to the top metallic contact. Inset: close-up of the mesa edge with a three-times larger color scale.

active region. This approximation allows one to use a sparser spatial mesh for the simulation and therefore reduce the computational power required. The resonator eigenmodes can be described by two mode numbers: the azimuthal number M (corresponding to the modulation of electric/magnetic fields as $e^{iM\theta}$ in the azimuthal direction) and the radial number N (which corresponds to the number of lobes of the eigenmodes in the radial direction). The four resonator modes of the small-size microdisks with frequencies closest to the material peak gain (≈2.6 THz) are shown in Figs. 3(a)–3(d). The mode resonance frequencies are spaced of ≈0.3 THz; thus only one mode can overlap with the material gain spectrum, whose full width at half maximum is ≈0.25 THz. This makes apparent the single-mode operation of our microcavity.

In order to quantify the effect of the thin n^+ top contact layers, a denser spatial mesh must be employed in the FE simulations, and reducing the required computational power becomes crucial. A 3D problem with axial symmetry can be mapped onto a numerically lighter two-dimensional (2D) problem with an integer parameter (the azimuthal number M), as it is explained in the very educational paper by Oxborrow.[19] The results [Figs. 3(e) and 3(f)] show that the presence of the n^+ top contact layer has a dramatic effect on the resonator modes. When the doped layer between the top metal border and the edge of the microdisk is present, the optical mode is guided by the surface plasmon at the active-region/n^+-layer interface [Fig. 3(e)]. The n^+ semiconductor layer is extremely lossy, and the calculated quality factor Q is 4. On the other hand, when this doped layer is removed, the resonator mode is bound to the metal. Not only is the optical mode more localized and not affected by the mesa sidewalls but the corresponding Q factor also increases ≈20 times, up to 90. Removing the n^+ top doped layer is therefore a crucial step. This result explains why our devices could reach the lasing regime only after this operation. The same argument can be applied to medium- and big-size microdisks.

In conclusion, we demonstrated single- and bimodal terahertz microcavity lasers with ultralow thresholds in the milliampere range ($I_{th}\approx 4$ mA) and with subwavelength mode volumes [$V_{eff}\approx 0.7\lambda_{effective}$ (Ref. 3)]. The emission wavelength is ≈114 μm, and the maximum operating temperatures are 70 and 60 K in pulsed and cw modes, respectively. The comparison with numerical simulations allows the identification of the resonator modes involved in the lasing process. The modes are guided by the top metallic layer. This peculiarity represents an additional degree of freedom in the design of terahertz resonators.

The authors thank I. Sagnes, S. Barbieri, and F. Julien for useful discussions. This work was conducted as part of a EURYI scheme award (www.esf.org/euryi) and partially supported through the EU project TeraNova. Device fabrication has been performed at the "Centrale Technologique Minerve" at the Institut d'Electronique Fondamentale.

[1] R. Köhler, A. Tredicucci, F. Beltram, H. E. Beere, E. H. Linfield, A. G. Davies, D. A. Ritchie, R. C. Iotti, and F. Rossi, Nature (London) **417**, 156 (2002).
[2] S. Kumar, S. Williams, Q. Hu, and J. L. Reno, Appl. Phys. Lett. **88**, 121123 (2006).
[3] S. M. Kim, F. Hatami, J. S. Harris, A. W. Kurian, J. Ford, D. King, G. Scalari, M. Giovannini, N. Hoyler, J. Faist, and G. Harris, Appl. Phys. Lett. **88**, 153903 (2006).
[4] C. Unterrainer, R. Colombelli, C. Gmachl, F. Capasso, H. Hwang, D. L. Sivco, and A. Y. Cho, Appl. Phys. Lett. **80**, 3060 (2002).
[5] B. Williams, S. Kumar, Q. Hu, and J. Reno, Opt. Express **13**, 3331 (2005), and references therein.
[6] S. Noda, Science **314**, 260 (2006).
[7] G. Bjork and Y. Yamamoto, IEEE J. Quantum Electron. **27**, 2386 (1991).
[8] R. Colombelli, C. Ciuti, Y. Chassagneux, and C. Sirtori, Semicond. Sci. Technol. **20**, 985 (2005).
[9] C. Ciuti, G. Bastard, and I. Carusotto, Phys. Rev. B **72**, 115303 (2005).
[10] C. Gmachl, F. Capasso, E. E. Narimanov, J. U. Nöckel, A. D. Stone, J. Faist, D. L. Sivco, and A. Y. Cho, Science **280**, 1556 (1998), and references therein.
[11] S. S. Dhillon, J. Alton, S. Barbieri, C. Sirtori, A. de Rossi, M. Calligaro, H. E. Beere, and D. A. Ritchie, Appl. Phys. Lett. **86**, 071107 (2005).
[12] V. Moreau, M. Bahriz, J. Palomo, L. R. Wilson, A. B. Krysa, C. Sirtori, D. A. Austin, J. W. Cockburn, J. S. Roberts, and R. Colombelli, IEEE Photonics Technol. Lett. **18**, 2499 (2006).
[13] C. Gmachl, F. Capasso, A. Tredicucci, D. L. Sivco, R. Kohler, A. L. Hutchinson, and A. Y. Cho, IEEE J. Sel. Top. Quantum Electron. **5**, 808 (1999).
[14] S. Johnson, P. Villeneuve, S. Fan, and J. Joannopoulos, Phys. Rev. B **62**, 8212 (2000).
[15] S. Barbieri, J. Alton, H. E. Beere, J. Fowler, E. H. Linfield, and D. A. Ritchie, Appl. Phys. Lett. **85**, 1674 (2004).
[16] Y. Chassagneux, J. Palomo, R. Colombelli, S. Barbieri, S. Dhillon, C. Sirtori, H. Beere, J. Alton, and D. Ritchie, Electronics Letters, in press.
[17] G. Fasching, A. Benz, C. Unterrainer, R. Zobl, A. M. Andrews, T. Roch, W. Schrenk, and G. Strasser, Appl. Phys. Lett. **87**, 211112 (2005).
[18] The simulations were performed with the commercial software package COMSOL MULTIPHYSICS.
[19] M. Oxborrow, e-print quant-ph/0607156 (2006).